ChemistrySelect

Research Article
doi.org/10.1002/slct.202203826

Chemistry Europe
European Chemical Societies Publishing

www.chemistryselect.org

Removal of Toxic Dyes and Paraquat by a Dual-Functional Metal-Organic Framework

Hai-Yan Sun[+],[a, b] Yu-Jie Gao[+],[a] Ji-Long Li,[a] Yan-Min Zou,[a] Mei-Ling Feng,*[a] and Xiao-Ying Huang[a]

Environmental contamination due to organic pollutants including organic dyes (*e.g.*, methylene blue (MB)) and paraquat (*i.e.*, methyl viologen (MV)) has become a serious problem. Herein, the removal for toxic cations of methylene blue (MB^+) and methyl viologen (MV^{2+}) has been realized by a three-dimensional (3D) anionic microporous metal-organic framework, namely $[Me_2NH_2][In(TDC)_2]\cdot 1.5DMA\cdot H_2O$ (FJSM-InMOF). FJSM-InMOF is capable of selectively adsorbing MB^+ in the presence of various dyes due to the effects of size-exclusion and charge-matching. Particularly, the strategy of combining adsorption and photocatalytic degradation realizes the thorough treatment of MB^+, which has been rarely reported. The adsorbent material can be easily regenerated and reused. Moreover, FJSM-InMOF exhibits a high capacity and rapid kinetics towards more toxic MV^{2+}. This work poses a new way for the selective removal of cationic organic pollutants and highlights the significance of combining different methods for the decontamination of organic pollutants.

Introduction

With the rapid development of industries and agricultures, the increase in the population and overexploitation of natural resources has brought about environmental problems of global concern over the past decades. Especially, the long-term residual accumulation of organic pollutants (such as organic dyes and herbicides) in the ecosystem may cause overall environmental hazards and even destroy the entire ecosystem.[1] Many dyes are considered as toxic, mutagenic and even carcinogenic environmental contaminants. For instance, acute inhaling of methylene blue (3,7-bis(dimethylamino)phenothiazin-5-ium chloride, abbreviated as MB) can cause shock, Heinz body formation, quadriplegia and tissue necrosis.[2] Meanwhile, the agrochemical paraquat (methyl viologen, 1,1-dimethyl-4,4-bipyridylium dichloride, abbreviated as MV) as a well-known herbicide is still frequently used worldwide though it has been forbidden in Europe.[3] MV is extremely toxic and mortal due to the generation of reactive radicals which could cause lesions in cellular membrane, protein and DNA.[4] Unfortunately, there is no specific antidote for MV toxicity. MV has brought about serious environment and food safety issues up to now.[5] However, it is rather difficult to efficiently remove them from solutions because of their high solubility, in the form of methylene blue cation (MB^+) and methyl viologen cation (MV^{2+}), respectively. Moreover, they are biologically non-degradable.

Numerous methods have been developed for the removal of dyes and paraquat from environment, such as coagulation,[6] membrane filtration,[7] adsorption,[8] photocatalytic degradation,[9] advance oxidation processes (AOP),[10] distillation, and electrolysis.[11] Among these methods, the adsorption technique is attractive because of its advantages such as high efficiency, easy operation of treating pollutants, simplicity of design and low cost.[12] Nowadays, a number of adsorbents have been reported to remove dyes and paraquat, such as activated carbon, silica, and polymer resins.[13] However, most of these adsorbents have poor selectivity for the removal of a particular organic dye, and generally are hard to regenerate.[6,14] Furthermore, most adsorbents remove pollutants just via concentration rather than mineralization to non-polluting substances, which might cause secondary pollution.[15] Photocatalysis is an effective approach for environmental remediation of organic pollutants with wide applicability, high decomposition efficiency, and recyclability of catalysts, which could mineralize organic pollutants under mild conditions without secondary pollution.[16] Undoubtedly, it is urgent to develop renewable materials with the ability of effective adsorption-enrichment and then photocatalytic degradation of organic pollutants. However, the combination of adsorption and photocatalytic degradation for the efficient removal of organic pollutants is still rare.[17]

Metal-organic framework (MOF) materials have presented excellent performance in the fields of adsorption, separation and storage of gases, catalysis, luminescence and so on.[18] MOFs have also been recognized as promising adsorbents for the removal of targeted dye pollutants due to their easy tunability of porosity and shape of the channel, exposed active sites and structural diversity.[18c,19] A few MOFs have demonstrated either adsorption or photodegradation capabilities

[a] *H.-Y. Sun,[+] Y.-J. Gao,[+] J.-L. Li, Y.-M. Zou, Prof. M.-L. Feng, Prof. X.-Y. Huang*
Department: State Key Laboratory of Structural Chemistry, Fujian Institute of Research on the Structure of Matter
Chinese Academy of Sciences
350001 Fu Zhou China
E-mail: fml@fjirsm.ac.cn
Homepage: http://www.fjirsm.ac.cn/research/R1/hxy/
[b] *H.-Y. Sun[+]*
University of Chinese Academy of Sciences
350001 Fu Zhou China
[+] *These authors contributed equally to this work.*

Supporting information for this article is available on the WWW under https://doi.org/10.1002/slct.202203826

toward MB^+ (Table S1). For example, Zn-MOF ($q_m = 326$ mg/g),[20] ZJU-71 ($q_m = 9.52$ mg/g)[21] and MOF-235 ($q_m = 252$ mg/g) exhibit superior performance for the removal of MB^+ by the adsorption method,[22] whereas MIL-53,[23] MIL-100(Fe),[24] Fe-BTC[24] and ZIF-8[25] present the outstanding catalytic degradation of MB^+. Up to now, however, only one MOF example of $\{[(CH_3)_2NH_2]_3(In_3L_4)\}\cdot(solvent)_x$ is documented to remove MB^+ by the combination of adsorption and photocatalysis method.[17,26] In addition, it is uncommon for MV^{2+} eliminated by MOFs[26] as exemplified by NKU-101 only.[11]

Herein, we report on the efficient decontamination of MB^+ and MV^{2+} from solutions with a dual-functional 3D anionic microporous framework, namely FJSM-InMOF ($[Me_2NH_2][In(TDC)_2]\cdot 1.5DMA\cdot H_2O$, H_2TDC = 2,5-thiophenedicarboxylic acid and DMA=N,N′-dimethylacetamide).[18c] Systematic studies reveal that FJSM-InMOF can selectively capture MB^+ from solutions even in the presence of interfering dye ions. More importantly, FJSM-InMOF presents highly efficient photocatalytic degradation for adsorbed MB^+ to achieve the thorough treatment of MB^+. The material can be reused once in an easy-to-operate and highly effective method. In addition, FJSM-InMOF also shows excellent removal performance for MV^{2+} with high adsorption capacity (56.03 mg/g). Our study shows effective and selective removal of both MV^{2+} and MB^+ by MOF materials via the rare combination of adsorption and photocatalysis, and resolves the problem of adsorption saturation and regeneration.

Results and Discussion

Structure of FJSM-InMOF

The pure crystalline sample of FJSM-InMOF could be easily synthesized in large scale through a one-pot solvothermal method (Figure 1a).[18c] FJSM-InMOF features a two-fold interpenetrated 3D microporous anionic framework of $[In(TDC)_2]_n^{n-}$ with diamond topology, in which there are channels with square cross sections of about 12.55×12.55 Å^2 that are filled with $[Me_2NH_2]^+$ cations, lattice water and DMA molecules (Figures 1b and 1c). The existence of exchangeable $[Me_2NH_2]^+$ combined with the high porosity of FJSM-InMOF implies that FJSM-InMOF is well-suited for ion exchange. Indeed, our previous study has confirmed the excellent ion exchange properties of FJSM-InMOF for the remediation of radioactive Cs^+ and Sr^{2+} ions.[18c]

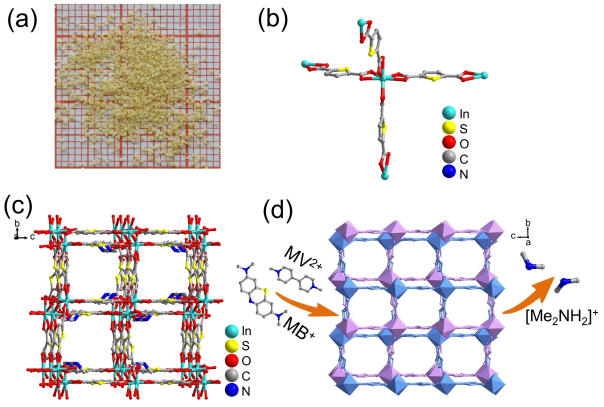

Figure 1. (a) Photograph of FJSM-InMOF crystals as synthesized without washing or manual selection. (b) Connection types of In^{3+} ion and TDC^{2-} ligands in FJSM-InMOF. (c) View of the 3D microporous framework of FJSM-InMOF along the *a*-axis; the lattice water and DMA molecules in the channels are omitted for clarity. (d) Schematic presentation of the capture of MB^+ and MV^{2+} cations by FJSM-InMOF through exchange of its $[Me_2NH_2]^+$ cations in the channels. For clarity, the $[Me_2NH_2]^+$ cations, lattice water, DMA molecules in the channels and hydrogen atoms are omitted.

Dyes Adsorption

Considering that FJSM-InMOF contains anionic open framework with high porosity and exchangeable cations in channels, we explored its potential application in removal of cationic organic pollutants. To check the adsorption ability of FJSM-InMOF towards cationic organic pollutants with different charges and sizes, various solutions of individual positively charged were prepared and treated by FJSM-InMOF, including MB^+, rhodamine B, crystal violet and 4-N,N-dimethylamino-4′-N′-methylstilbazolium ($[DAMS]^+$), positively and negatively charged brilliant blue G, uncharged sudan I, and negatively charged methyl orange and orange II. The adsorption abilities of FJSM-InMOF for the above organic pollutants were evaluated by the UV-Vis spectroscopy with the inset photographs highlighting the color change of dye solution (Figure 2) with increasing contact time. According to Figures 2a and 2b, the UV adsorption peaks of MB^+ and $[DAMS]^+$ at 654 and 480 nm disappeared in the presence of FJSM-InMOF after 48 hours, respectively, corresponding to the color change of solutions from blue or red to colorless.[27] It was monitored that the color of rhodamine B solution had slight decolorization under the presence of FJSM-InMOF according to the gentle dropping of the maximum adsorption band at 543 nm (Figure 2c).[28] Nevertheless, negligible change has been observed under the same experimental conditions for the UV peaks at the maximum adsorption wavelength of 588, 609, 477, 416 and 481 nm for crystal violet, brilliant blue G, sudan I, methyl orange and orange II solutions, respectively (Figures 2d-2 h).[29] Correspondingly, the color of solutions of these dyes didn't change under the presence of FJSM-InMOF. The above results show that FJSM-InMOF (the cross section of channel: 12.55×12.55 Å^2) can selectively adsorb cationic MB^+ (with the size of 13.4×5.0×4.3 Å^3) (Table S2) and $[DAMS]^+$ (with the size of 13.7×4.2×1.9 Å^3), while it exhibits poor adsorption ability for cationic rhodamine B (with the slightly larger size 15.9×11.8×5.6 Å^3) (Figure S3) and no adsorption for cationic crystal violet (with the larger size 17.2×15.8×15.8 Å^3). Meanwhile, it is found that FJSM-InMOF could not adsorb anionic (brilliant blue G, methyl orange, orange II) and neutral (sudan I) dyes. These results indicate that the adsorption performance of FJSM-InMOF is related to the size and charge of organic dyes. The adsorption of cationic organic dyes with relatively small size, *e.g.*, MB^+ and $[DAMS]^+$ should originate from the size of channels in FJSM-InMOF, anionic microporous framework and exchangeable $[Me_2NH_2]^+$ cations in channels, which can be well explained by

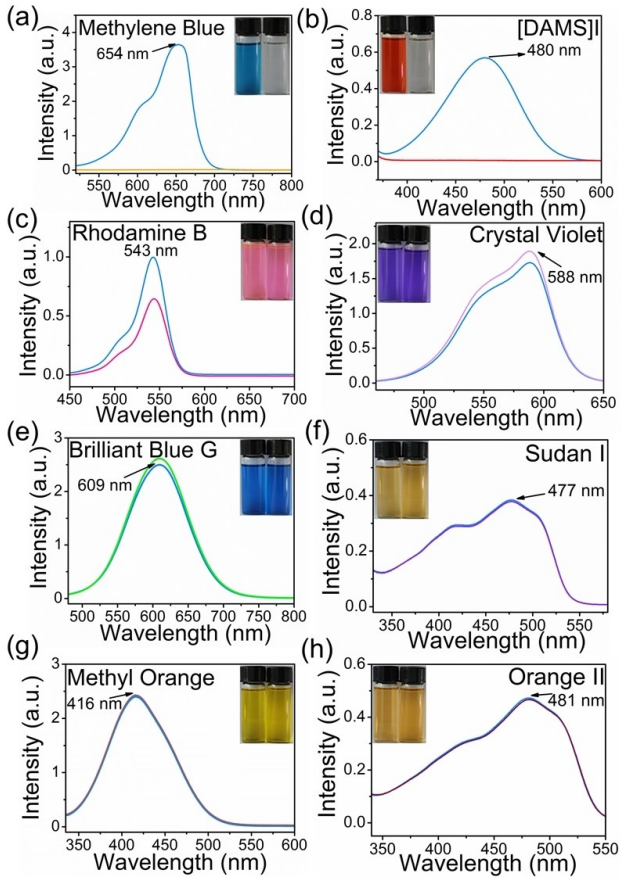

Figure 2. The UV-Vis spectra and photographs of various dyes solutions before (left) and after (right) adsorption by FJSM-InMOF: MB^+ (a), $[DAMS]^+$ (b), rhodamine B (c), crystal violet (d), brilliant blue G (e), sudan I (f), methyl orange (g) and orange II (h), respectively (V/m = 1000 mL/g, RT (~25 °C), contact time = 48 h).

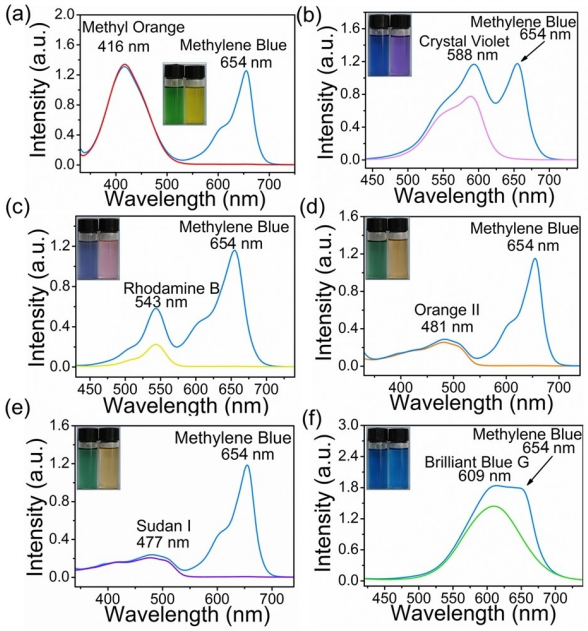

Figure 3. Sequential UV-Vis spectral changes of mixed solutions with various dyes: MB/methyl orange (a), MB/crystal violet (b), MB/rhodamine B (c), MB/orange II (d), MB/sudan I (e) and MB/brilliant blue G (f), respectively (V/m = 1000 mL/g, RT ~25 °C, contact time = 48 h). Inset is the corresponding photograph of solutions before (left) and after (right) the adsorption.

the size-exclusion effect and charge-matching effect.[30] It would be more practical if FJSM-InMOF could selectively adsorb specific dye in solutions containing different dyes.

Therefore, the selective MB^+ adsorption performance of FJSM-InMOF as the representative was explored in detail. As shown in Figure 3, the competitive adsorption experiments of MB^+ by FJSM-InMOF in the presence of other interfering dye have been carried out. When FJSM-InMOF was immersed in a mixed solution of MB^+ and methyl orange, the characteristic peak of methyl orange at 416 nm had almost no change, whereas the characteristic peak of MB^+ at 654 nm completely disappeared, along with the color change of solution from green to yellow (Figure 3a). When crystal violet was selected as the competitive dye, the color of solution changed from blue to violet, and the characteristic peak of crystal violet at 588 nm slightly decreased while the peak of MB^+ at 654 nm decreased drastically (Figure 3b). The color of the mixed solution of rhodamine B and MB^+ changed significantly from blue to pink as the peak of rhodamine B at 543 nm was weakened, while that of MB^+ at 654 nm disappeared (Figure 3c). For the solution with mixed orange II and MB^+, the intensity of UV peak at 481 nm ascribed to orange II remained unchanged, and the peak at 654 nm ascribed to MB^+ was not found. As a result, the color of solution markedly changed from green to yellow (Figure 3d). In Figure 3e, the maximum adsorption peak of Sudan I at 477 nm was maintained, while the peaks of MB^+ vanished (654 nm), which made the solution undergo distinct color change from green to yellow. Besides, when brilliant blue G competed with MB^+, the UV peak of brilliant blue G solution at 609 nm was kept and the peak of MB^+ at 654 nm was absent (Figure 3f). Correspondingly, the color of solution changed from dark blue to light blue. The above results indicate that FJSM-InMOF holds the excellent selective adsorption capability for MB^+ even under the various interfering dyes. Thus, FJSM-InMOF may be considered as a fascinating material for the separation of MB^+ from other dye ions.

Then the kinetics of FJSM-InMOF for MB^+ adsorption was investigated. UV-Vis spectra showed that the typical absorbance bands of MB^+ at 654 nm were weakened significantly over time. As shown in Figure 4 and Table S2, the concentration of MB^+ ion (~14 ppm) rapidly decreased in 30 minutes and the removal rate reached 52.28%. And the adsorption rate of MB^+ was close to 100% after 12 hours and the residual MB^+ in the solution was below 0.05 ppm. Therefore, FJSM-InMOF presents rapid and comparatively exhaustive adsorption for MB^+. The kinetic data of MB^+ adsorption are well fitted with the pseudo-second order kinetic model with $R^2 = 0.99664$; that is, the plot of t/q_t vs t shows a perfect linear relation.

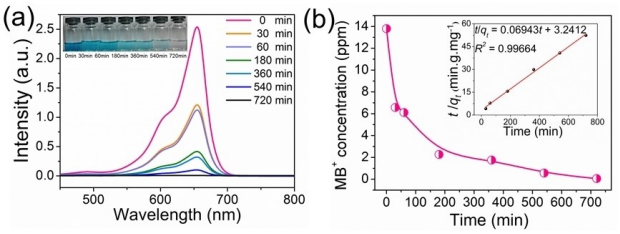

Figure 4. (a) The UV-Vis spectral changes of MB^+ solution in the presence of FJSM-InMOF at different time intervals. The inset photographs show color changes of MB^+ solutions in adsorption. (b) Kinetic curves of MB^+ adsorption by FJSM-InMOF. Insets: the plots of t/q_t vs t (with the initial concentration about 14 ppm, $V/m = 1000$ mL/g, RT ~25 °C, shading).

Photocatalytic Degradation of MB^+ by FJSM-InMOF and Reuse of FJSM-InMOF

To evaluate the photodegradation capabilities of FJSM-InMOF for MB^+, the adsorption spectra of MB^+ solution in the presence of FJSM-InMOF under UV-light irradiation were investigated with increasing contact time (Figure 5a). To ensure adsorption equilibrium, FJSM-InMOF was adequately immersed in the MB^+ solution in the dark (named MB-FJSM-InMOF), and then exposed to UV light.

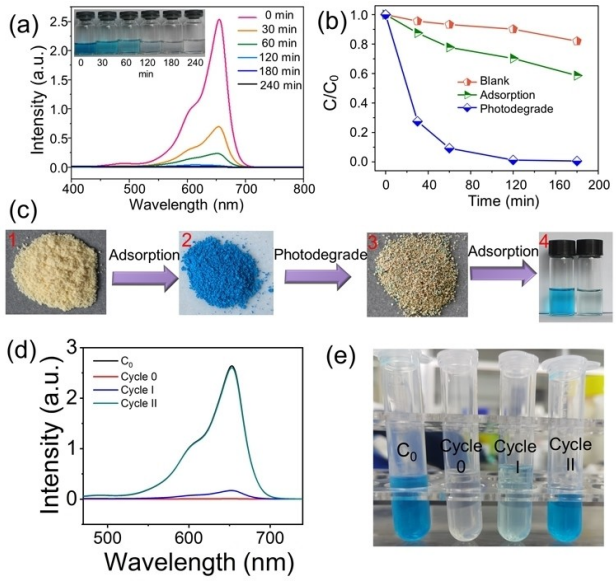

Figure 5. (a) UV spectra of MB^+ photodegradation by MB-FJSM-InMOF at the different time intervals. Inset: photograph showing the color change of MB^+ solutions. (b) Degradation ratio curves of MB^+ adsorption by FJSM-InMOF under different conditions (blue line: under UV irradiation; green line: shading condition, $V/m = 1000$ mL/g); the blank test was conducted with MB^+ solution under UV irradiation without FJSM-InMOF (yellow line). (c) Photographs of FJSM-InMOF (1), the products of MB^+-adsorbed FJSM-InMOF (2), the MB^+ degradation product from MB^+-adsorbed sample after irradiation under UV-light for 48 h (3), and photographs of MB^+ solutions before (left) and after (right) MB^+ adsorbed by degradation products of 3 for 12 h (4). (d) UV-Vis spectra of MB^+ solutions in the presence of FJSM-InMOF in Cycle 0, Cycle I, and Cycle II experiments (The initial concentration of MB^+ is about 10 ppm; RT ~25 °C; 12 hrs). (e) Photographs showing the color of MB^+ solutions in cycle experiments (The initial concentration of MB^+ is about 10 ppm; $V/m = 1000$ mL/g; RT ~25 °C; C_0: initial concentration).

Obviously, the characteristic peak of MB^+ at 654 nm disappeared and the color of solution (blue) faded rapidly under the irradiation of UV-light for 3 hours (Figure 5a). Moreover, the concentration of MB^+ solution dramatically decreased from 2.536 to 0.235 ppm at 60 minutes, and the concentration declined to 0.015 ppm within 3 hours (Table S3). This indicates that the MB-FJSM-InMOF has higher removal efficiency for MB^+ under photocatalysis than solely adsorption. In order to exclude the influence of adsorption and self-degradation of MB^+, the performances of MB^+ adsorption by MB-FJSM-InMOF without UV-light and blank tests were compared (Figure S4). The UV peaks of MB^+ solution were maintained under shading test and blank test (Figure S4). This indicates that the self-degradation of MB^+ and adsorption by MB-FJSM-InMOF in dark can be neglected (Figure 5b). This confirms that FJSM-InMOF could efficiently and catalytically photodegrade MB^+ under UV light.

In practical industrial applications, it is important to investigate the recyclability and stability of the catalyst, and the recycling method should be as simple as possible.[31] Herein, we used an easy-to-operate and highly effective method to recycle FJSM-InMOF. As shown in Figure 5c, the color of MOF changed from yellow to blue after the adsorption of MB^+. Astonishingly, the color of MB^+-adsorbed products changed from blue to yellow after irradiation under UV-light for 48 h (Figure 5c-3), which implied FJSM-InMOF might be regenerated effectively by UV-light. The color of the MB^+ solution changed from blue to almost colorless under the regeneration of FJSM-MOF for 24 h (Figure 5c-4), indicating that the recovered products could still remove MB^+. Indeed, PXRD pattern and SEM images (Figure S2) of MB^+-adsorbed products indicated that there was no structural and crystalline degradation after the treatment with MB^+, revealing that FJSM-InMOF exhibited excellent stability during the process of adsorption and photodegradation of MB^+. Figure 5d presents the UV spectra of MB^+ solutions in the cycle experiments, in which "Cycle 0" curve refers to the UV-Vis spectrum for the MB^+ methanol solution after adding the pristine FJSM-InMOF, "Cycle I" curve is UV-Vis spectrum of the MB^+ solution after adding the MB^+-adsorbed product in Cycle 0 after UV irradiation, and "Cycle II" is the UV-Vis spectrum of the MB^+ solution after adding the MB^+-adsorbed product in Cycle 1 after UV irradiation. In cycle II, the color of solution turned back to blue implying that the regenerated material almost lost adsorption capacity (Figure 5e). According to PXRD, the framework of material is no longer maintained after the cycle II experiment, as shown in Figure S5, which could result in the degeneration of MB^+ adsorption performance for FJSM-InMOF.

In a word, FJSM-MOF showed high stability during the processes, and it could also be recycled after being used as adsorbent and photocatalyst, which might reduce the overall cost of adsorbent material.

Adsorption of Paraquat

Adsorption kinetics of FJSM-InMOF for MV^{2+} ions were investigated at RT (Figure 6). The UV adsorption peaks of MV^{2+} were centered at 261 nm (Figure 6a). As shown in Figures 6a and 6b, it was obvious that the UV absorption peak of MV^{2+} at 261 nm was weakened significantly over time. The concentrations of MV^{2+} (~12 ppm) rapidly decreased, corresponding to the removal rate of more than 80% for MV^{2+} within 24 hours and about 90% within 48 hours (Figure 6b and Table S4). The pseudo-second order kinetic model also could fit the MV^{2+} kinetic data well with $R^2 = 0.99425$, and the plot of t/q_t vs t for kinetics data showed a perfect linear relation.

To further confirm the uptake capacity of FJSM-InMOF towards MV^{2+}, isotherm experiments were performed by testing the UV adsorption peaks of MV^{2+}. The equilibrium adsorption data of MV^{2+} with various concentrations are well fitted with Langmuir adsorption isotherm model with $R^2 = 0.9731$ (Figure 6c and Table S5). The fitting results with the Langmuir adsorption model show that the maximum exchange capacity q_m of FJSM-InMOF is 56.03 mg/g for MV^{2+}. It is worth noting that the uptake capacity of FJSM-InMOF for MV^{2+} is higher than that of most known adsorption materials (Figure 6d, Table 1), such as silica modified with titania (13.68 mg/g),[32] amberlite resins (9.8 mg/g)[33] and insoluble cyclodextrin polymer (26.7 mg/g).[34] It shows FJSM-InMOF has the great adsorption ability toward trapping toxic MV^{2+}, which has been rarely reported for the removal of MV^{2+} by MOF materials.

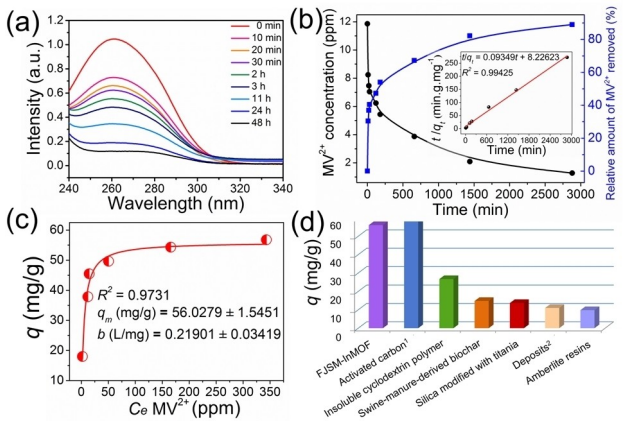

Figure 6. (a) UV spectra of MV^{2+} adsorption by FJSM-InMOF at different time. (b) Kinetic curves of MV^{2+} adsorption by FJSM-InMOF plotted as the concentration (ppm) (black line) and the relative amount removed (%) (blue line) *vs* the time t (min), respectively. Insets: the plots of t/q_t vs t. (c) MV^{2+} equilibrium curves for FJSM-InMOF ($V/m = 1000$ mL/g, RT ~25 °C). (d) Comparison of MV^{2+} removal efficiency with other reported materials (1: Activated carbon derived from used tires.[13a] 2: Deposits from drinking water networks.[3] Insoluble cyclodextrin polymer.[34] Swine-manure-derived biochar.[35] Silica modified with titania.[32] Amberlite resins.[33]).

Removal Mechanism for MB^+ and MV^{2+}

PXRD patterns of FJSM-InMOF before and after adsorption and photocatalysis for MB^+ are shown in Figure S6a, which confirms the complete structural transformation from *Pccn* to $P4_122$ as indicated by the disappearance of (110) and (242) diffraction peaks. The intrusion of MB^+ ions into FJSM-InMOF breaks the structural centrosymmetry and results in the generation of chiral structure of FJSM-InMOF-MB. This change is consistent with our previous work of In-MOF for removing Cs^+ and Sr^{2+} ions, which has been clarified to be the ion-exchange mechanism.[18c] The result is also confirmed by elemental analysis (EA). EA for the products of FJSM-InMOF: C, 37.97%; H, 3.99%; N, 5.69%; found: C, 36.46%; H, 4.36%; N, 5.31%. EA for the products of FJSM-InMOF after adsorption of MB^+: C, 31.14%; H, 2.98%; N, 2.50%. And EA for the products of FJSM-InMOF after adsorption of $[DAMS]^+$: C, 32.81%; H, 3.20%; N, 2.73%. Meanwhile, PXRD patterns of FJSM-InMOF before and after adsorption of MV^{2+} are shown in Figure S6b, which coincides with PXRD patterns of FJSM-InMOF after adsorption of MB^+. The adsorption results indicate that the cross section of channels in FJSM-InMOF with the size of 12.55×12.55 Å^2 is suitable for adsorption of both MB^+ ($13.4 \times 5.0 \times 4.3$ Å^3) and MV^{2+} ($10.7 \times 5.32 \times 4.1$ Å^3).

Conclusion

In summary, we have developed an efficient and recyclable dual-functional FJSM-InMOF material to remove MB^+ and

Table 1. The comparison of MB^+ and MV^{2+} removal efficiencies by various adsorbents in this work and references.

Materials	Ions	Equilibrium time	q_m (mg/g)	Mechanism	Refs
FJSM-InMOF	MB^+	12 h	–	Ion exchange, Photocatalytic Degradation	this work
FJSM-InMOF	MV^{2+}	24 h	56.03	Ion exchange	this work
Fe^{II}@MIL-100(Fe)	MB^+	–	–	Photocatalytic Degradation	[36]
MOF-235	MB^+	–	–	Adsorption	[22]
$[(CH_3CH_2)_2NH_2]_{1/2}[Zn(BTC)_2/_3(PyC)_{1/4}]\cdot$solvent (NKU-101)	MV^{2+}	16 h	160	Adsorption	[11]
Insoluble cyclodextrin polymer	MV^{2+}	–	26.7	Adsorption	[34]
Silica modified with titania	MV^{2+}	–	13.68	Adsorption	[32]
Amberlite resins	MV^{2+}	–	9.8	Adsorption	[33]
deposits from drinking water networks	MV^{2+}	–	11	Adsorption	[3]
activated carbon derived from used tires	MV^{2+}	–	61	Adsorption	[13a]
Swine-manure-derived biochar	MV^{2+}	–	14.8	Adsorption	[35]

(H_2PyC = 4-pyrazolecarboxylic acid; H_3BTC = 1,3,5-benzenetricarboxylic acid.)

MV^{2+}. It is indicated that the strategy of combination for adsorption and photocatalytic degradation is effective for thorough treatment of MB^{+} by FJSM-InMOF. In addition, the reason that FJSM-InMOF could selectively adsorb MB^{+} in the presence of interfering dyes is attributed to the size-exclusion effect and charge-matching effect as well as free and exchangeable $[Me_2NH_2]^{+}$ cations in FJSM-InMOF. Prominently, MB^{+}-adsorption product can be recovered by an easily operated and highly effective method (under UV-light irradiation) and the recollected FJSM-InMOF still exhibits good adsorption capacity for MB^{+}, which is rare for MOF materials. FJSM-InMOF can resolve the problem of adsorption saturation and regeneration, achieving a long-term cycle utilization of adsorption material. The excellent adsorption performance of FJSM-InMOF is also reflected in its high adsorption capacity towards MV^{2+} (56.03 mg/g). This work provides the basis for additional applications in size- and charge-selective ion chromatography and the paraquat elimination by MOFs.

Experimental Section

FJSM-InMOF was synthesized using $In(NO_3)_3{\cdot}4.5H_2O$ and H_2TDC in 4 mL N,N′-dimethylacetamide (DMA) by the solvothermal method at 150 °C as we previously reported.[18c] Element analysis (EA) of C, H, and N were conducted on a German Elementary Vario EL III instrument. Powder X-ray diffraction (PXRD) patterns were collected on a Miniflex II diffractometer using Cu$K\alpha$ ($\lambda = 1.54178$ Å) at 30 kV and 15 mA in the angular range of $2\theta = 5$–$55°$ at room temperature (RT). Simulated PXRD patterns were generated by using the single crystal X-ray structural data via Mercury software. Scanning electron microscope (SEM) images were obtained on the JEOL JSM-6700F scanning electron microscope. All UV/Vis spectra were measured on Shimadzu 2600 UV-Vis spectrophotometer at RT.

Supporting Information Summary

Details about synthesis, ion exchange experiments, concentration standard curves of MB^{+} and MV^{2+}, EDS diagrams, the summary of MOFs materials sorbents related to the adsorption and/or catalytic degradation of MB^{+}, and tables with experimental specific data are provided in supporting information.

Acknowledgements

This work was supported by the National Natural Science Foundations of China (grant nos. U21A20296, 22076185 and 21771183), the Natural Science Foundation of Fujian Province (grant no. 2020J06033).

Conflict of Interest

The authors declare no conflict of interest.

Data Availability Statement

The data that support the findings of this study are available in the supplementary material of this article.

Keywords: Adsorption · Metal-organic framework · Organic dye · Paraquat · Photocatalytic degradation

[1] a) M. T. Uddin, M. A. Islam, S. Mahmud, M. Rukanuzzaman, *J. Hazard. Mater.* **2009**, *164*, 53–60; b) M. A. Al-Ghouti, M. A. M. Khraisheh, S. J. Allen, M. N. Ahmad, *J. Environ. Manage.* **2003**, *69*, 229–238.
[2] a) S. Chakrabarti, B. K. Dutta, *J. Colloid Interface Sci.* **2005**, *286*, 807–811; b) R. M. Gong, M. Li, C. Yang, Y. Z. Sun, J. Chen, *J. Hazard. Mater.* **2005**, *121*, 247–250; c) K. V. Kumar, V. Ramamurthi, S. Sivanesan, *J. Colloid Interface Sci.* **2005**, *284*, 14–21; d) K. C. Chen, J. Y. Wu, C. C. Huang, Y. M. Liang, S. C. J. Hwang, *J. Biotechnol.* **2003**, *101*, 241–252.
[3] M. S. F. Santos, G. Schaule, A. Alves, L. M. Madeira, *Chem. Eng. J.* **2013**, *229*, 324–333.
[4] Q. Zhao, S. H. Li, R. L. Chai, X. Ren, C. Zhang, *ACS Appl. Mater. Interfaces* **2020**, *12*, 7504–7509.
[5] a) R. Betarbet, T. B. Sherer, G. MacKenzie, M. Garcia-Osuna, A. V. Panov, J. T. Greenamyre, *Nat. Neurosci.* **2000**, *3*, 1301–1306; b) A. Walcarius, R. Mouchotte, *Arch. Environ. Contam. Toxicol.* **2004**, *46*, 135–140.
[6] B. Shi, G. Li, D. Wang, C. Feng, H. Tang, *J. Hazard. Mater.* **2007**, *143*, 567–574.
[7] J. W. Lee, S. P. Choi, R. Thiruvenkatachari, W. G. Shim, H. Moon, *Water Res.* **2006**, *40*, 435–444.
[8] D. Mahanta, G. Madras, S. Radhakrishnan, S. Patil, *J. Phys. Chem. B* **2008**, *112*, 10153–10157.
[9] J. Fernandez, J. Kiwi, C. Lizama, J. Freer, J. Baeza, H. D. Mansilla, *J. Photochem. Photobiol. A* **2002**, *151*, 213–219.
[10] W. Chen, W. Lu, Y. Yao, M. Xu, *Environ. Sci. Technol.* **2007**, *41*, 6240–6245.
[11] Y. Y. Jia, Y. H. Zhang, J. Xu, R. Feng, M. S. Zhang, X. H. Bu, *Chem. Commun.* **2015**, *51*, 17439–17442.
[12] a) Y. C. Wong, Y. S. Szeto, W. H. Cheung, G. McKay, *Langmuir* **2003**, *19*, 7888–7894; b) H. Tamai, T. Yoshida, M. Sasaki, H. Yasuda, *Carbon* **1999**, *37*, 983–989.
[13] a) N. K. Hamadi, S. Swaminathan, X. D. Chen, *J. Hazard. Mater.* **2004**, *112*, 133–141; b) G. Mezohegyi, F. P. van der Zee, J. Font, A. Fortuny, A. Fabregat, *J. Environ. Manage.* **2012**, *102*, 148–164; c) J. Roosen, J. Spooren, K. Binnemans, *J. Mater. Chem. A* **2014**, *2*, 19415–19426; d) Y. Zhang, Y. Li, L. Q. Yang, X. J. Ma, L. Y. Wang, Z. F. Ye, *J. Hazard. Mater.* **2010**, *178*, 1046–1054.
[14] a) Y. Al-Degs, M. A. M. Khraisheh, S. J. Allen, M. N. Ahmad, *Water Res.* **2000**, *34*, 927–935; b) Y. Yu, Y. Y. Zhuang, Z. H. Wang, M. Q. Qiu, *Ind. Eng. Chem. Res.* **2003**, *42*, 6898–6903; c) Y. C. He, J. Yang, W. Q. Kan, H. M. Zhang, Y. Y. Liu, J. F. Ma, *J. Mater. Chem. A* **2015**, *3*, 1675–1681.
[15] J. Yang, D. Chen, Y. Zhu, Y. Zhang, Y. Zhu, *Appl. Catal. B* **2017**, *205*, 228–237.
[16] a) C. Chen, W. Ma, J. Zhao, *Chem. Soc. Rev.* **2010**, *39*, 4206–4219; b) M. Wen, G. Li, H. Liu, J. Chen, T. An, H. Yamashita, *Environ. Sci.-Nano* **2019**, *6*, 1006–1025.
[17] Q. Li, D. X. Xue, Y. F. Zhang, Z. H. Zhang, Z. Gao, J. Bai, *J. Mater. Chem. A* **2017**, *5*, 14182–14189.
[18] a) D. Farrusseng, S. Aguado, C. Pinel, *Angew. Chem. Int. Ed.* **2009**, *48*, 7502–7513; b) J. R. Li, R. J. Kuppler, H. C. Zhou, *Chem. Soc. Rev.* **2009**, *38*, 1477–1504; c) Y. J. Gao, M. L. Feng, B. Zhang, Z. F. Wu, Y. Song, X. Y. Huang, *J. Mater. Chem. A* **2018**, *6*, 3967–3976; d) D. Sheng, L. Zhu, C. Xu, C. Xiao, Y. Wang, Y. Wang, L. Chen, J. Diwu, J. Chen, Z. Chai, T. E. Albrecht-Schmitt, S. Wang, *Environ. Sci. Technol.* **2017**, *51*, 3471–3479; e) B. Parmar, K. K. Bisht, G. Rajput, E. Suresh, *Dalton Trans.* **2021**, *50*, 3083–3108; f) U. Patel, B. Parmar, P. Patel, A. Dadhania, E. Suresh, *Mater. Chem. Front.* **2021**, *5*, 304–314; g) U. Patel, B. Parmar, A. Dadhania, E. Suresh, *Inorg. Chem.* **2021**, *60*, 9181–9191.
[19] I. Ahmed, S. H. Jhung, *Chem. Eng. J.* **2017**, *310*, 197–215.
[20] J. Zhang, F. Li, Q. Sun, *Appl. Surf. Sci.* **2018**, *440*, 1219–1226.
[21] X. Duan, J. Yu, Q. Zhang, Y. Cui, Y. Yang, G. Qian, *Mater. Lett.* **2016**, *185*, 177–180.
[22] E. Haque, J. W. Jun, S. H. Jhung, *J. Hazard. Mater.* **2011**, *185*, 507–511.
[23] J. J. Du, Y. P. Yuan, J. X. Sun, F. M. Peng, X. Jiang, L. G. Qiu, A. J. Xie, Y. H. Shen, J. F. Zhu, *J. Hazard. Mater.* **2011**, *190*, 945–951.
[24] F. Martinez, P. Leo, G. Orcajo, M. Diaz-Garcia, M. Sanchez-Sanchez, G. Calleja, *Catal. Today* **2018**, *313*, 6–11.
[25] H. P. Jing, C. C. Wang, Y. W. Zhang, P. Wang, R. Li, *RSC Adv.* **2014**, *4*, 54454–54462.

[26] S. Rojas, P. Horcajada, *Chem. Rev.* **2020**, *120*, 8378–8415.
[27] Y. A. Cheng, W. F. Liu, Y. B. Yan, H. M. Zhou, *Protein Pept. Lett.* **2006**, *13*, 125–128.
[28] T. A. Khan, M. Nazir, E. A. Khan, *Toxicol. Environ. Chem.* **2013**, *95*, 919–931.
[29] a) C. Sahoo, A. K. Gupta, A. Pal, *Dyes Pigm.* **2005**, *66*, 189–196; b) S. U. Jadhav, M. U. Jadhav, A. N. Kagalkar, S. P. Govindwar, *J. Chin. Inst. Chem. Eng.* **2008**, *39*, 563–570; c) A. Su, Q. Zhong, Y. Chen, Y. Wang, *Anal. Chim. Acta* **2018**, *1023*, 115–120; d) S. Anandan, P. Sathishkumar, N. Pugazhenthiran, J. Madhavan, P. Maruthamuthu, *Sol. Energy Mater. Sol. Cells* **2008**, *92*, 929–937.
[30] a) C. P. Li, H. Zhou, S. Wang, H. H. Yuan, S. Z. Zhang, M. Du, *Chem. Commun.* **2017**, *53*, 4767–4770; b) S. Tian, S. Xu, J. Liu, C. He, Y. Xiong, P. Feng, *J. Cleaner Prod.* **2019**, *239*; c) V. K. M. Au, S. Y. Kwan, M. N. Lai, K. H. Low, *Chem. Eur. J.* **2021**, *27*, 9174–9179.
[31] Y. Jiao, Y. Liu, F. Qu, A. Umar, X. Wu, *J. Colloid Interface Sci.* **2015**, *451*, 93–100.
[32] W. T. Tsai, K. J. Hsien, Y. M. Chang, C. C. Lo, *Bioresour. Technol.* **2005**, *96*, 657–663.
[33] M. P. Leite, L. G. T. dos Reis, N. F. Robaina, W. F. Pacheco, R. J. Cassella, *Chem. Eng. J.* **2013**, *215*, 691–698.
[34] J. Junthip, W. Promma, S. Sonsupap, C. Boonyanusith, *Iran. Polym. J.* **2019**, *28*, 213–223.
[35] W. T. Tsai, H. R. Chen, *Int. J. Environ. Sci. Technol.* **2013**, *10*, 1349–1356.
[36] H. Lv, H. Zhao, T. Cao, L. Qian, Y. Wang, G. Zhao, *J. Mol. Catal. A* **2015**, *400*, 81–89.

Submitted: September 30, 2022
Accepted: November 18, 2022